The Role of Visible Data in Improving Satellite Rain-Rate Estimates

PATRICK W. S. KING AND WILLIAM D. HOGG

Environment Canada, Downsview, Ontario, Canada

PHILLIP A. ARKIN

National Meteorological Center, Washington, D.C.

(Manuscript received 27 April 1994, in final form 8 December 1994)

ABSTRACT

Data from the first Algorithm Intercomparison Project (AIP/1) collected over Japan and surrounding waters in June, July, and August 1989 are used in this study to assess the importance of visible data in satellite rain estimation techniques. The purpose of the project was to compare different methods for estimating rainfall using satellite measurements. Radar and surface gauge data provided the validation set.

RAINSAT, an estimation technique using both visible (VIS) and infrared (IR) data, achieved the highest correlation with the validation data. In this paper rainfall estimates from RAINSAT (VIS + IR) are compared with two IR-only techniques to deduce the effectiveness of VIS data. Some estimates are also made using a VIS-only technique. Comparisons are made on both a spatial and diurnal basis.

Cloud climatologies for a subset of the AIP/1 data and the southern Ontario data on which RAINSAT was trained showed a marked similarity. It is found that the total volume of rain as a function of albedo is very similar for both Japanese and Ontario data.

The VIS data generally produced higher correlations with the validation data than did the IR data. This was especially the case when rain fell from warm, orographically induced rainfall. When rain fell from cold bright clouds, especially over the ocean, the correlations of the two types of data with the validation data were similar.

It is also shown that normalization of VIS data by the cosine of solar zenith data was inadequate to remove diurnal variations in apparent brightness.

1. Introduction

The World Climate Research Programme established the Global Climatology Project (GPCP) to provide climate researchers with global precipitation statistics for the period 1986–95. Within the GPCP a series of Algorithm Intercomparison Projects have been conducted to evaluate different algorithms for estimating rainfall using satellite measurements and to identify reasons for differences among the different techniques.

The first Algorithm Intercomparison Project (AIP/1) occurred over Japan and surrounding waters from 1 June to 30 June and 15 July to 15 August 1989. The Japanese Meteorological Agency (JMA) provided hourly visible (VIS) and Infrared (IR) data from the Geostationary Meteorological Satellite (GMS). Special Sensor Microwave/Imager (SSM/I) data were provided by a United States military satellite (DMSP). After estimates were submitted, the participating groups were provided with validating data consisting of composites of radar and rain gauge data. The area of validating data is indicated by the lettered boxes shown in Fig. 1. Satellite data were available for a larger area bounded by 22.5°–46.25°N, 120°–147°E.

Fifteen groups from six countries submitted 27 different algorithms. Seventeen algorithms used IR or VIS/IR data and 10 used SSM/I data. The estimates for AIP/1 were assessed at a workshop held in Washington, D.C., in May 1991. The results were summarized in Lee et al. (1991) and further discussed by Arkin and Xie (1994). Grassotti and Garand (1994) indicated the usefulness of visible data in their study with AIP/1 data.

One result of the workshop was that RAINSAT, a VIS–IR technique trained using radar data from southern Ontario, showed a higher correlation for daily rainfall accumulation than did IR-only techniques. RAINSAT had the highest correlation with validation data and the lowest root-mean-square error (rmse) for the June period (see Table 5.3 in Lee et al. 1991). In the July–August period it had the highest correlation but only the ninth lowest rmse. Arkin and Xie (1994) point out that the differences in correlation between the methods are significant if the data are assumed to

Corresponding author address: Patrick W. King, Atmospheric Environment Service, Environment Canada, 4905 Dufferin St., Downsview, Ontario, M3H 5T4 Canada.

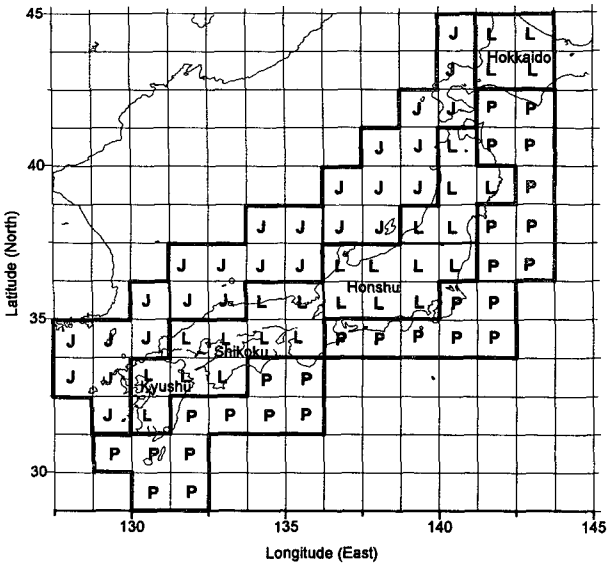

FIG. 1. The study area of GPCP AIP/1. The lettered boxes indicate grids for which validation data from a combination of radar and gauge data were available; "J" refers to grids over the Sea of Japan, "P" to Pacific Ocean grids, and "L" to grids over land.

be independent. When the number of degrees of freedom are decreased to take into consideration the spatial and serial correlation of the data, the differences in correlation become less significant. In addition, as will be shown later, significant diurnal variations may be masked by using daily results.

Negri and Adler (1993) discussed the performance of three satellite IR-only rainfall techniques using the AIP/1 dataset. They found that all three techniques did poorly in estimating the rain maxima on the southeast coast of Japan. The GOES precipitation index (GPI—to be discussed later) isolated a broad maximum in the correct location for June but not July/August.

The purpose of this note is to assess the reasons for the improved performance of the VIS–IR algorithm in making daily estimates relative to IR-only algorithms.

We do this by making comparisons between RAINSAT and the GOES precipitation index (GPI) (Arkin and Meisner 1987). We chose GPI since it represents a de facto standard for IR-only techniques, being the algorithm used by the GPCP for rain estimates in the Tropics. Comparisons are made between rain-rate maps produced by these two techniques and the verification dataset for the entire day and for day and night separately. We also compare hourly correlations between the two estimates and the verification set. All of this analysis is based on estimates submitted prior to the receipt of the verification data.

To assess the contributions of the VIS and IR data separately, we made comparisons during daylight hours only of the daytime RAINSAT algorithm (VIS + IR), the nighttime RAINSAT algorithm (IR-only), and a VIS-only estimate.

2. Methods used

a. RAINSAT

RAINSAT is a supervised classification procedure that is trained to recognize precipitating clouds using radar observations. In the original version (Lovejoy and Austin 1979) a probability matrix was constructed to relate GOES VIS–IR pairs to probability of precipitation (PoP). This was later modified to produce rain rate using a third-degree polynomial relationship between PoP and rain rate (Hogg 1990; Garand 1989).

For AIP/1 a VIS–IR rain-rate matrix was constructed directly from a training set consisting of two summers (June, July, and August) of GOES and corresponding weather radar data from southern Ontario (King 1990). This matrix was smoothed using a spline filter and is shown in Fig. 2a. It can be seen that there is more dependence on the VIS than the IR since

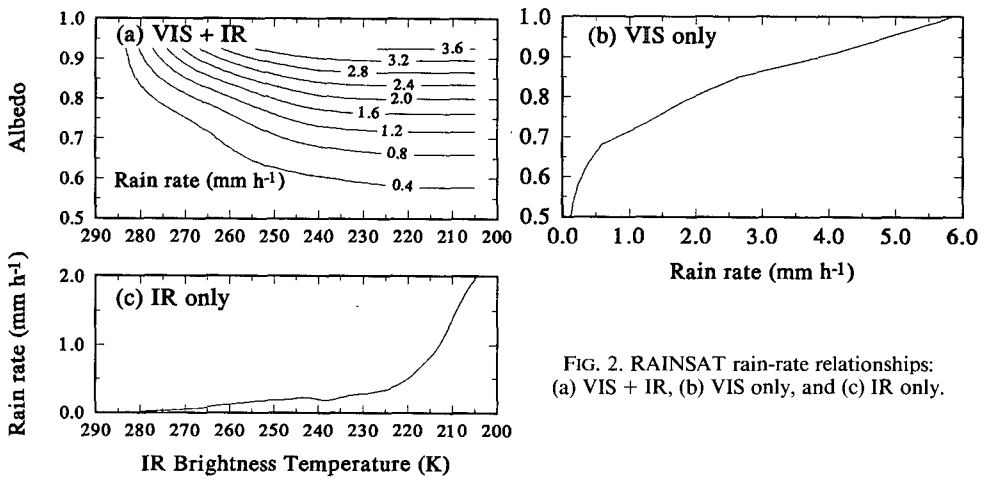

FIG. 2. RAINSAT rain-rate relationships: (a) VIS + IR, (b) VIS only, and (c) IR only.

changes are more rapid for a given change in VIS than IR. It can also be noted that the rain rate changes very rapidly for albedos greater than 0.7.

The VIS-only (Fig. 2b) and IR-only (Fig. 2c) rain-rate relationships were interpolated from the actual data without smoothing. The VIS-only relationship shows no significant rainfall for albedos less than 0.5 and rapidly increasing rain rates for albedos greater than 0.7. The IR-only relationship shows a rapid increase in rain rate for temperatures colder than 220 K.

b. GPI

As described by Arkin and Meisner (1987), the GPI is an IR temperature threshold technique that assumes that all pixels colder than 235 K precipitate at a constant rate of 3 mm h^{-1}. Note that this is significantly greater than the RAINSAT IR-only algorithm that reaches 1 mm h^{-1}. GPI is the IR algorithm currently used by the GPCP for rainfall estimation in the Tropics.

3. Data used

a. Southern Ontario

The data used in calibrating the RAINSAT algorithm and for the comparisons in this study were collected during June, July, and August of 1987 and 1988. Radar data at a resolution of 2 km × 2 km were collected over the area within 100 km of King radar (44.0°N, 79.6°W) near Toronto. About 80% of the study area was land. Collocated *GOES-7* satellite data were collected and remapped to 8 km × 8 km on a Lambert conformal projection. The radar pixels were averaged to reduce the resolution to the same as the satellite data.

The GOES VIS data were normalized for sun angle by dividing by square root of cos(SZA), where SZA is the solar zenith angle, and converted to albedo using coefficients calculated by William Rossow for the International Satellite Cloud Climatology Project (ISCCP) (Rossow and Schiffer 1991). The square root is necessary since the normalization was done on the VIS counts, which are related to the square root of the incident radiant power (Minnis and Harrison 1984). VIS data were accumulated in bins 0.04 wide in albedo and the IR data in bins 4 K wide in equivalent brightness temperature.

b. Japan

The data for Japan consisted of VIS and IR data from GMS mapped to a 0.05° latitude by 0.0625° longitude grid (approximately 5 km × 5 km) for the area shown in Fig. 1. The VIS data had already been converted to albedo, and the IR data were in the form of equivalent blackbody brightness temperatures. The validating data was provided by JMA and consisted of rain-rate maps derived from AMeDAS (Automated Meteorological Data Acquisition System) radar and rain gauges and was mapped to the same grid. Verification was limited to the Japanese Islands and adjacent water covered by radar as outlined in Fig. 1. About 65% of the area for which verification data were available was over water. According to Lee et al. (1991) the radars are turned off when no rain is observed and a check is then made 3 h later. Based on limited testing they decided to treat all missing data as zero rainfall. We followed this procedure in our analysis. As will be seen later, grid squares distant from land seem to suffer from underestimated rainfall.

The GMS VIS data are nominal albedos and were normalized for sun angle by dividing each value by cos(SZA). To assess the efficacy of the normalization data, we constructed histograms of both normalized and unnormalized VIS data for each hour of the June period of AIP/1. We calculated the albedo at every 10th percentile from 10% to 90%. If there are no diurnal trends and the cosine normalization is effective, the normalized curve should be a horizontal straight line.

The 90th percentile curves, representing the brightest clouds, for the unnormalized and normalized data are shown in Fig. 3. Two facts are immediately apparent: there is a morning–afternoon asymmetry in the unnormalized data and the normalized curve shows a rising trend with a peak two hours after local noon. Similar patterns were noted for more restricted areas (5° latitude by 5° longitude) and even for a single grid square on a day with fairly uniform heavy rain.

The 1400 JST maximum could be due to a diurnal trend, to shortcomings in the normalization, or perhaps

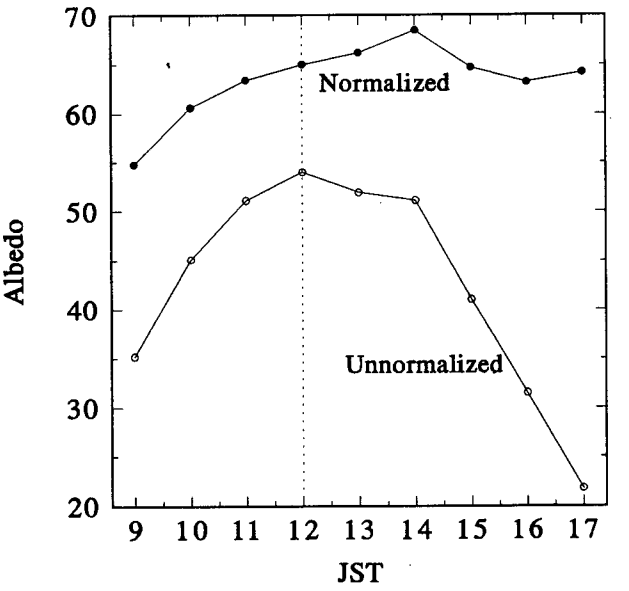

FIG. 3. The 90th percentile of brightness for normalized and unnormalized pixels for AIP/1 June 1989.

a combination of the two. Given that GMS was stationed at 140°E near the central longitude of the study area (133.5°E), one would expect minimal morning–afternoon asymmetries due to the satellite–sun geometry (Minnis and Harrison 1985). It is much beyond the scope of this paper to attempt to answer this question.

We believe that the upward turn in the normalized curve at 1700 JST is an artefact due to the normalization. The normalization factors are about 3 at this time, which can result in an amplification of errors.

4. Results

a. Cloud climatologies in Japan and southern Ontario

As noted earlier, the RAINSAT rain-rate relationship was derived using data from southern Ontario. No adjustments were made to apply RAINSAT to Japan. Thus, in assessing RAINSAT rain estimates for AIP/1, it will be useful to compare the cloud climatologies for southern Ontario and for Japan during AIP/1.

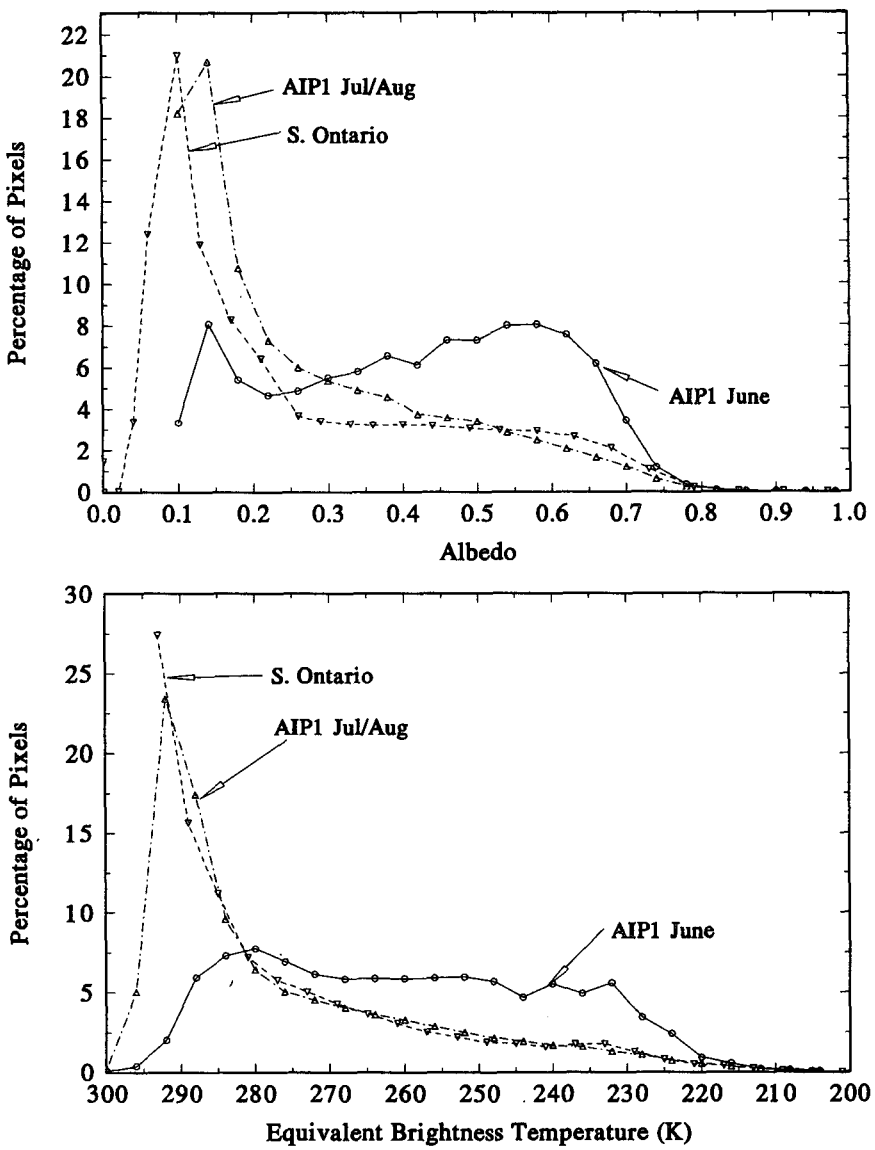

FIG. 4. (a) The distribution of pixels as a function of albedo. Data have been accumulated in bins 0.04 wide: ○—AIP/1 1–30 June data, △—AIP/1 15 July–15 August data, and ▽—southern Ontario data. (b) The distribution of pixels as a function of equivalent brightness temperatures. Data have been accumulated in bins 4 K wide. All pixels warmer than 291 K for the southern Ontario data are grouped in one bin. The three curves are labeled as in Fig. 2a.

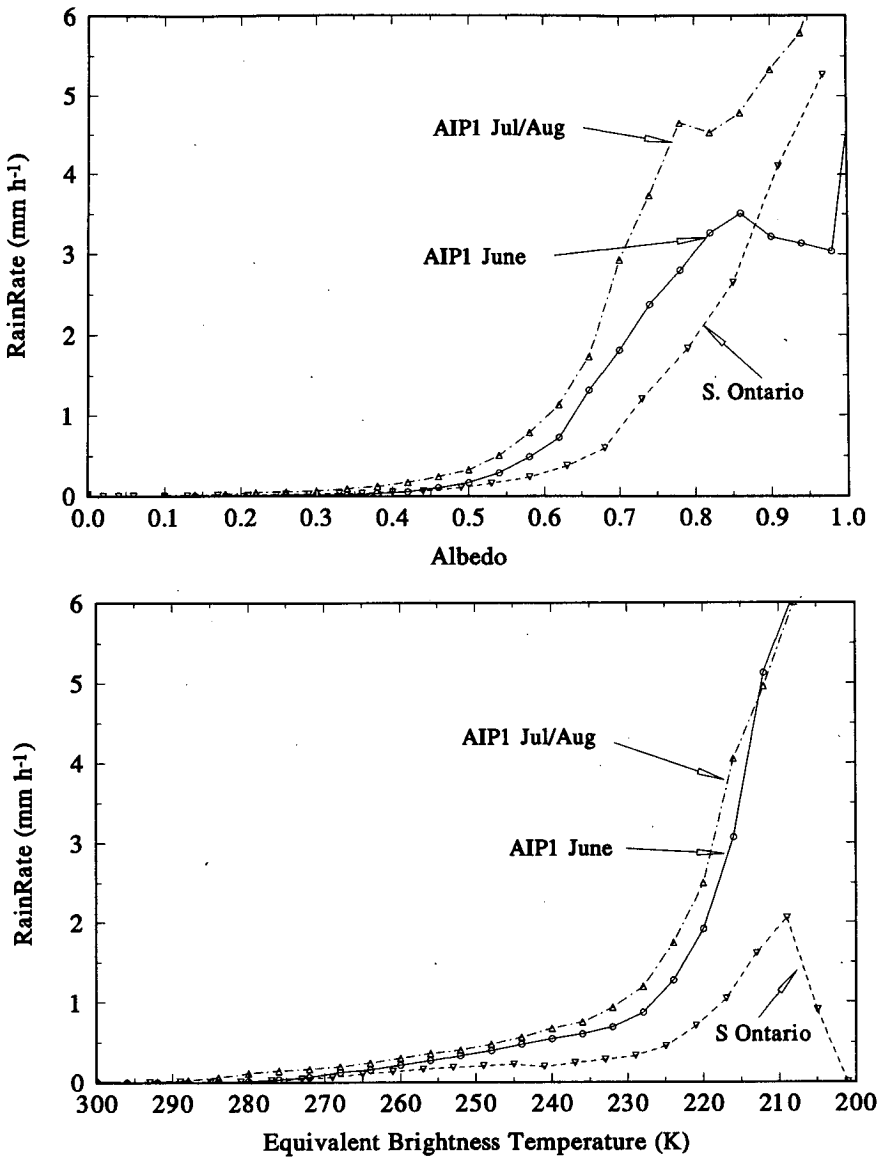

FIG. 5. (a) Rain rate as a function of albedo. The same bins and labels as in Fig. 2a apply. (b) Rain rate as a function of equivalent brightness temperature. The same bins and labels as in Fig. 2b apply.

There are large differences between the climates of southern Ontario and Japan. The climate of southern Ontario in the summer is largely continental in nature with a slight maritime influence from the Great Lakes. Most summer rain falls as showers and thunderstorms with a maximum in late afternoon. The mean monthly precipitation is about 75 mm in each of June, July, and August (Hare and Thomas 1979). The topography of southern Ontario is flat to gently rolling and as a result orographic effects are small.

The Baiu period in Japan (June) is characterized by frequent heavy rainfalls from a subtropical stationary front along the boundary between a tropical air mass and a midlatitude air mass (Ninomiya and Akiyama 1971). The mid-July to mid-August period is characterized by a monsoonal circulation. Most of the rain falls from convective clouds (Fukui 1977) and there are occasional typhoons. Monthly rainfall during the Baiu period ranges from 200 to 400 mm in southern Honshu, Kyushu, and Shikoku to 75–100 mm in Hokkaido (JMA 1993). Thus the rain rates in southern Japan are three to five times higher than in southern Ontario for the same time period. In the July–August period, rainfall amounts are similar in the south and increase in the north (JMA 1993). In

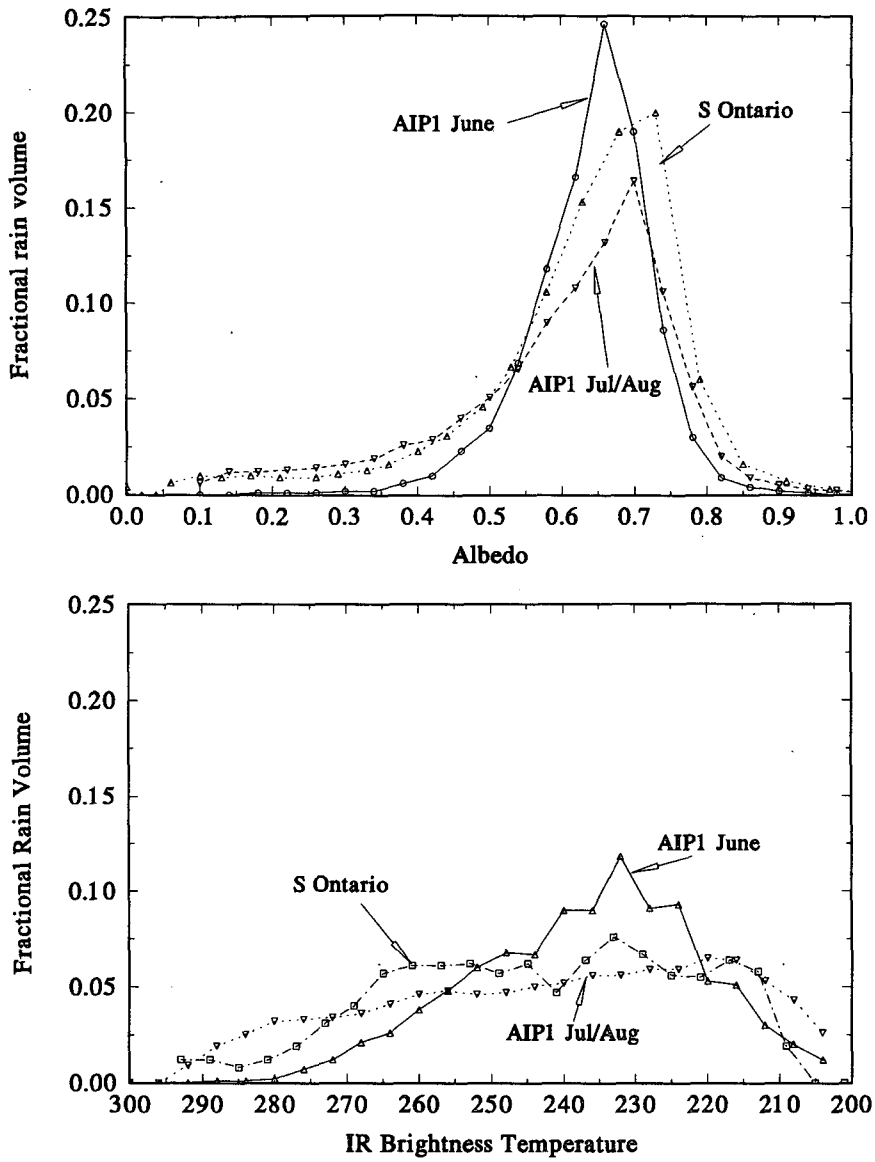

FIG. 6. (a) Fractional rain volume as a function of albedo. The same bins and labels as in Fig. 2a apply. (b) Fractional rain volume as a function of equivalent brightness temperature. The same bins and labels as in Fig. 2b apply.

the second period there is a pronounced orographic effect as slopes facing the Pacific receive much more rain than those facing the Sea of Japan (JMA 1993).

Fujibe (1988) found a pronounced afternoon maximum in convective precipitation during summer months at inland stations throughout Japan. For coastal stations, the maximum in convective precipitation tended to be from 0300 to 0600 JST, with stations on the southeast coast tending toward the latter time. For widespread precipitation there was a weak maximum throughout Japan in the early to mid-morning.

Given the apparently large difference in climates between southern Ontario and Japan, it is interesting to compare the characteristics of the RAINSAT training sample and the AIP/1 validation set. Figures 4a and 4b show the percentage of pixels observed for each albedo and equivalent brightness temperature category, respectively. The total number of pixels for southern Ontario was about 1 million; it was about 6 million for AIP/1 June, and about 8.5 million for AIP/1 July/August.

The most striking feature is the similarity between the southern Ontario data and the July–August period

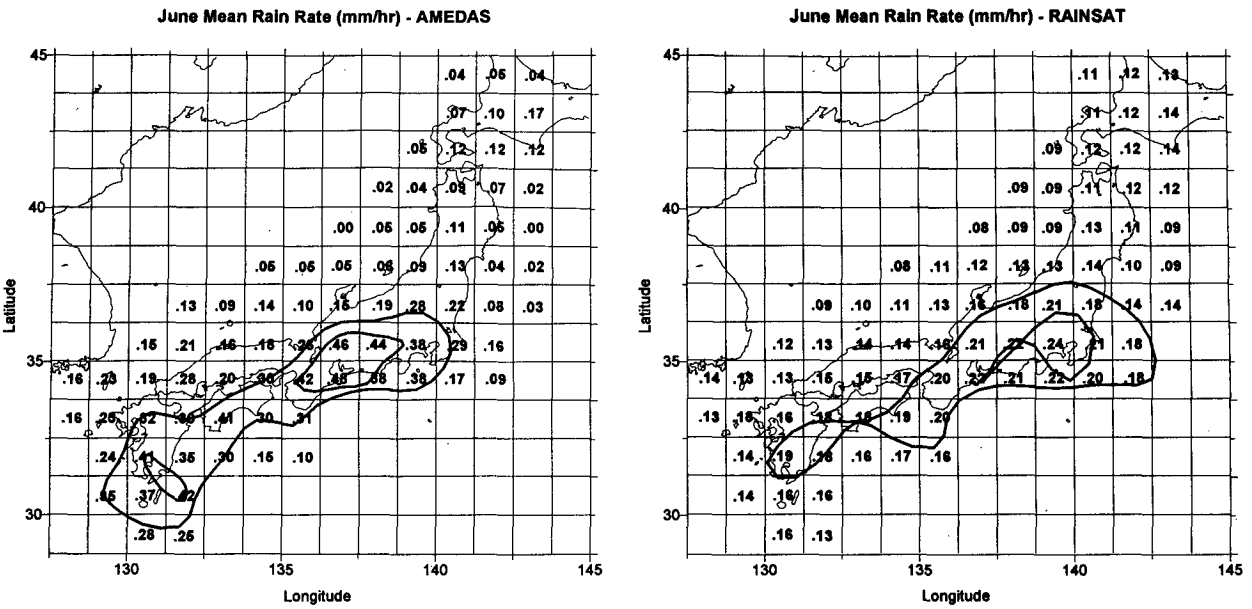

FIG. 7. (a) AMeDAS mean rain rate (mm h^{-1}) for AIP/1 June 1989. (b) RAINSAT mean rain rate (mm h^{-1}) for AIP/1 June 1989.

of AIP/1. In both cases there is a very strong peak at an albedo of 0.10–0.15 in the VIS and near 290 K in the IR. This of course is due mainly to cloud-free areas. The difference in the peak may be due to differences in surface albedos or may indicate a difference in the intercalibration between GOES and GMS. At the higher albedos typical of clouds the distributions are broadly similar; at colder temperatures, the distributions are almost exactly the same. The convective cloud regimes that prevail at these times in southern Ontario and near Japan result in remarkably similar distributions of cloud albedos and brightness temperatures.

The AIP/1 June data has quite different characteristics. There is a broad but pronounced peak of clouds from warm (stratus) to cold (cirrus). There is a weak peak about 280 K in the IR and at 0.15 in the VIS, which presumably represents relatively cloud-free areas. The cloud climatology during the Baiu obviously is very different from the Ontario clouds and also the July–August period.

Rain rate as a function of albedo and brightness temperature is shown in Figs. 5a and 5b, respectively. The rain rates in southern Ontario are much lower than either of the Japanese datasets. The IR relationship shows much the same rain-rate relationship for both Japanese datasets. In the VIS case, the July–August dataset shows considerably higher rain rates for a given albedo than does the June dataset.

For all three datasets, the rain rate increases markedly for albedos greater than 0.6 (VIS) and at temperatures colder than 230 K (IR). When we compare with the histograms in Fig. 4, we see that there are very few pixels with these temperatures and albedos. To see the effect of changes in VIS and IR on the total rainfall, we define the fractional rain volume. The fractional rain volume for the jth category (FRV_j) is a nondimensional number that shows the proportion of the total rain that falls in each category. It is defined as

$$FRV_j = \frac{RR_j N_j}{\sum_i RR_i N_i},$$

where RR_j is the rain rate and N_j is the number of occurrences for the jth category.

By definition the sum over all categories must be 1.

The fractional rain volume for VIS data are illustrated in Fig. 6a. The three curves show the average for the two summers in Ontario and for each of the two periods of AIP/1. There is a remarkable similarity among the three curves. All show rapidly increasing volumes of rain for clouds with albedos greater than 0.5 reaching peak volumes for albedos in the 0.65–0.75 range. During the Baiu period of AIP/1, 25% of the rain fell for albedos in the range 0.63–0.66 and over 60% in the range from 0.59 to 0.71.

Similar curves for the IR are shown in Fig. 6b. The distribution of rain volume with brightness temperature is much less peaked than for albedo, with only one value exceeding 10%. The June period of AIP/1 does exhibit greater peakedness, with more than 40% of the rain volume occurring for brightness temperatures from 220 to 245 K, while the July–August period of AIP/1 and the Ontario data both display a flat distribution showing no great dependence of rain volume on IR brightness temperature.

Based on these data it appears that there is a fairly similar relationship between rainfall and cloud albedo in southern Ontario and Japan, despite the different climates. The cloud climatologies calculated using IR data show a reasonable correspondence between the monsoonal convective regime in Japan and the continental convective regime in Ontario. Of course these are based on average relationships, and very different relationships may occur when we look at restricted subsets of the data.

b. *Spatial variations*

Maps showing the average hourly rain rate for the June period are shown for AMeDAS and RAINSAT in Figs. 7a and 7b, respectively. Each box is the average of 720 hourly estimates. There is a maximum in rain along the southeast Japanese coast. RAINSAT captures the location of this maximum but it overestimates the rain in Hokkaido. Note that we have drawn contours to highlight the location of the relative maximum in each case and that the actual maximum values are quite different.

Similar maps for July/August are shown in Figs. 8a and 8b. Each box is an average of 762 hourly values. The AMeDAS data show strong maxima along the southeast coast; one centered near the coast of central Honshu, the other on the main southern islands of Shikoku and Kyushu. The RAINSAT estimates are very low and do not show a great deal of variation. There is, however, a maximum in the right place on the central Honshu coastline.

To assess the contribution of the VIS, we produced similar maps for daylight hours only. These are shown for June in Figs. 9a (AMeDAS) and 9b (RAINSAT). Similarly July/August is shown in Figs. 10a and 10b. In June the maximum in RAINSAT is more pronounced than is the case for the entire 24-h period. In July/August the maximum along the southeast coast is more clearly present in the RAINSAT product than is the case in Fig. 8b.

In the next section we will discuss these diurnal tendencies in some detail.

c. *Diurnal variations using the RAINSAT and GPI algorithms*

To assess the contribution of the VIS data to the RAINSAT estimates, average rain rates and correlation coefficients between the rainfall estimates and validation data were calculated for each hour of the day for all 62 days of AIP/1. The hourly correlations were done simply by grouping all data for a given hour assuming spatial and day to day independence. The resulting diurnal variation curves for RAINSAT, GPI, and AMeDAS are discussed below.

Figure 11a shows mean hourly rain rates for June averaged over all marked grid squares from Fig. 1 for AMeDAS, RAINSAT and GPI. Each value represents the average of the results of 2370 1.25° boxes.

The AMeDAS shows a relatively constant rain rate for all hours. GPI is relatively constant but there is a broad maximum in late afternoon and a broad minimum near midnight. RAINSAT on the other hand is

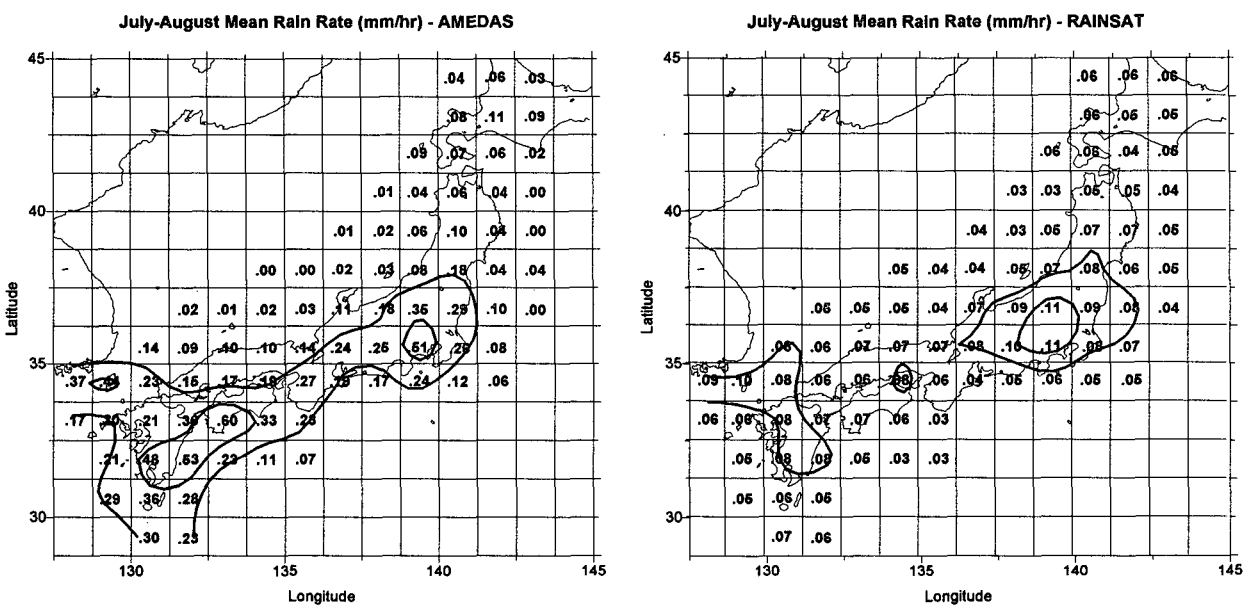

FIG. 8. (a) AMeDAS mean rain rate (mm h^{-1}) for AIP/1 July–August 1989. (b) RAINSAT mean rain rate (mm h^{-1}) for AIP/1 July–August 1989.

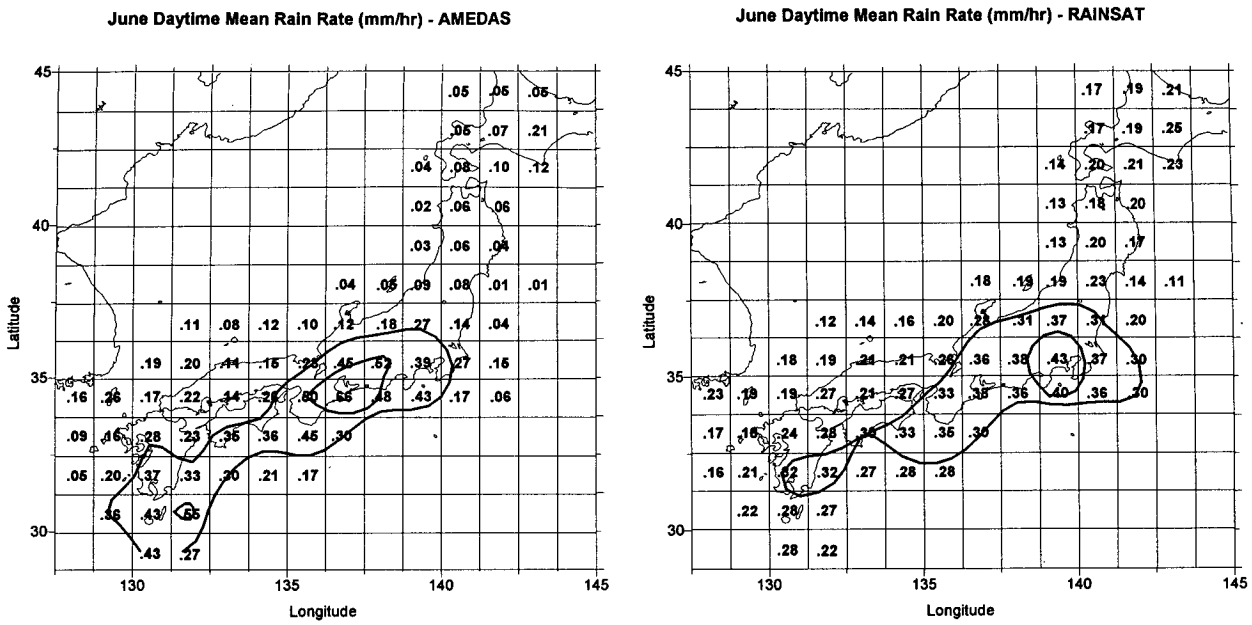

FIG. 9. (a) AMeDAS mean rain rate (mm h^{-1}) for AIP/1 June 1989 for daylight hours only. (b) RAINSAT mean rain rate (mm h^{-1}) for AIP/1 June 1989 for daylight hours only.

constant at night but shows a rising rain rate until early afternoon and then remains relatively steady. The shape of the RAINSAT curve is exactly the same as that for the 90th percentile of brightness shown in Fig. 3. Thus, this variation must be due to increasing reflectivity (either apparent or real) in the VIS. This points to an inadequacy in normalizing the VIS data. Obviously from Figs. 4 and 5, the rain rate and rain volume are extremely sensitive to small changes in brightness for the very brightest clouds. More work is

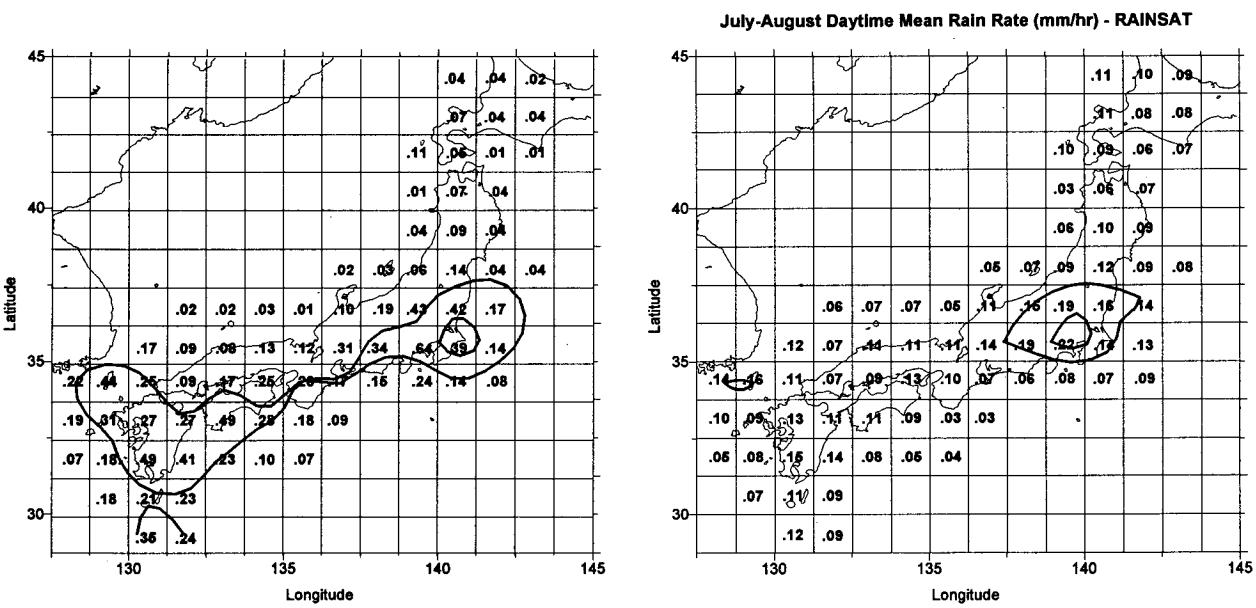

FIG. 10. (a) AMeDAS mean rain rate (mm h^{-1}) for AIP/1 July–August 1989 for daylight hours only. (b) RAINSAT mean rain rate (mm h^{-1}) for AIP/1 July–August 1989 for daylight hours only.

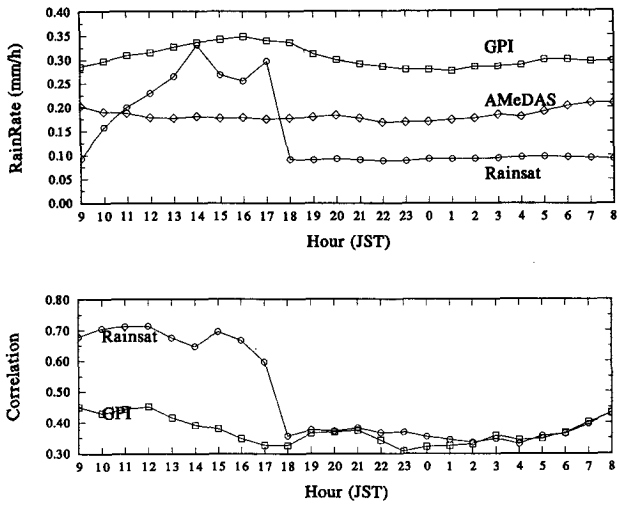

FIG. 11. (a) Average rain rates averaged over the whole study area for each hour in AIP/1 1–30 June. The AMeDAS verification data are represented by diamonds, the GPI by squares, and RAINSAT by circles. (b) Correlation between GPI (□) and RAINSAT (○) and AMeDAS. The correlations were done by grouping all AIP/1 grid squares together without regard for location.

needed on VIS normalization if VIS data are to be used from different satellites and different geographical areas.

The correlation with the AMeDAS data for both RAINSAT and GPI (Fig. 11b) shows that RAINSAT has a much higher correlation with AMeDAS for all daylight hours and is of course very similar to GPI at night when both methods use only IR data. Applying Fisher's Z transformation shows that differences in correlation coefficient of approximately 0.02 or more are significant at the 95% confidence level.

Figure 12a is similar to Fig. 11a but for 15 July to 15 August. The AMeDAS data show a slight increase in rain rate to a weak maximum in the midafternoon and then a slow decline to a broad minimum in the evening and rises again to a broad maximum about 0400 JST. The GPI shows a similar diurnal variation but with greater amplitude. RAINSAT again shows identical shape during daylight hours as in June but with much lower rain rates. Again it remains at a lower, constant value at night.

Figure 12b again shows increased correlation for RAINSAT in the daytime due to the use of VIS data. However, there is a definite diurnal trend. Both RAINSAT and GPI decrease in correlation with AMeDAS data from a maximum in the early daylight hours to a minimum just after (RAINSAT) and just before (GPI) sunset. They both then rise to a secondary maximum about local midnight and fall to a secondary minimum just before sunrise. The diurnal trend in daylight hours will be discussed in the next section. The superiority of GPI at night contrasts with the almost identical behavior of the two techniques in the June dataset. This pattern might be explained if most of the raining clouds were in the range from 220 to 235 K.

d. Regional variations in diurnal trends

There is a strong variation in rainfall over the Japanese Islands during the warm months as is evident from Figs. 7a and 8a and from Fujibe (1988). To see how this affects the diurnal variations, we calculated mean rain rates and correlations for a VIS + IR technique, an IR-only technique and a VIS-only technique for grid boxes lying predominantly over land (L in Fig. 1), the Pacific Ocean (P), and the Sea of Japan (J). The results are shown for June in Fig. 13 and for July/August in Fig. 14.

In June the diurnal AMeDAS rain rates are similar for grids over land and over the Pacific; rain rates are much lower over the Sea of Japan. The VIS + IR and VIS-only methods have similar results for land and the Pacific both showing the same pattern as the 90th percentile from Fig. 3. Over the Sea of Japan the estimates are lower but not nearly as much lower as they should be. The IR-only is nearly steady over land and the Pacific and much too low. Over the Sea of Japan it is slightly lower and very nearly the same as AMeDAS. In the correlations some interesting patterns emerge. Over the Pacific all three methods have similar correlations in the morning, but the VIS + IR and VIS-only rise in the afternoon while the IR-only falls slightly. Over land the VIS + IR and VIS-only correlations decline slightly through the day but the IR-only declines markedly. Over the Sea of Japan all the correlations are lower but the IR-only is very low throughout the entire

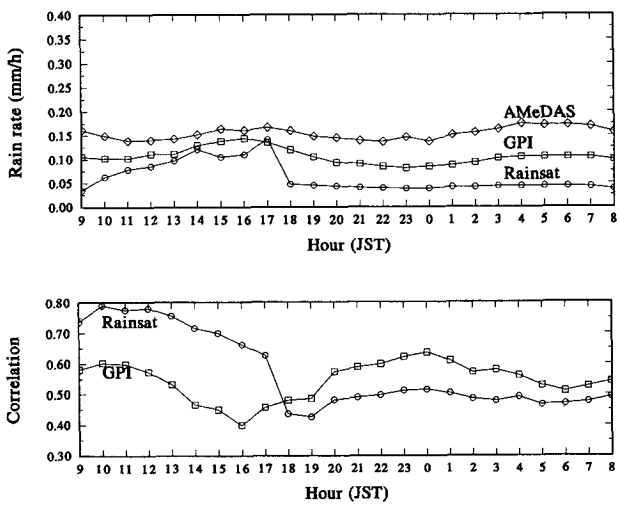

FIG. 12. (a) As Fig. 5a but for AIP/1 15 July–15 August 1989. (b) As Fig. 5b but for AIP/1 15 July–15 August 1989.

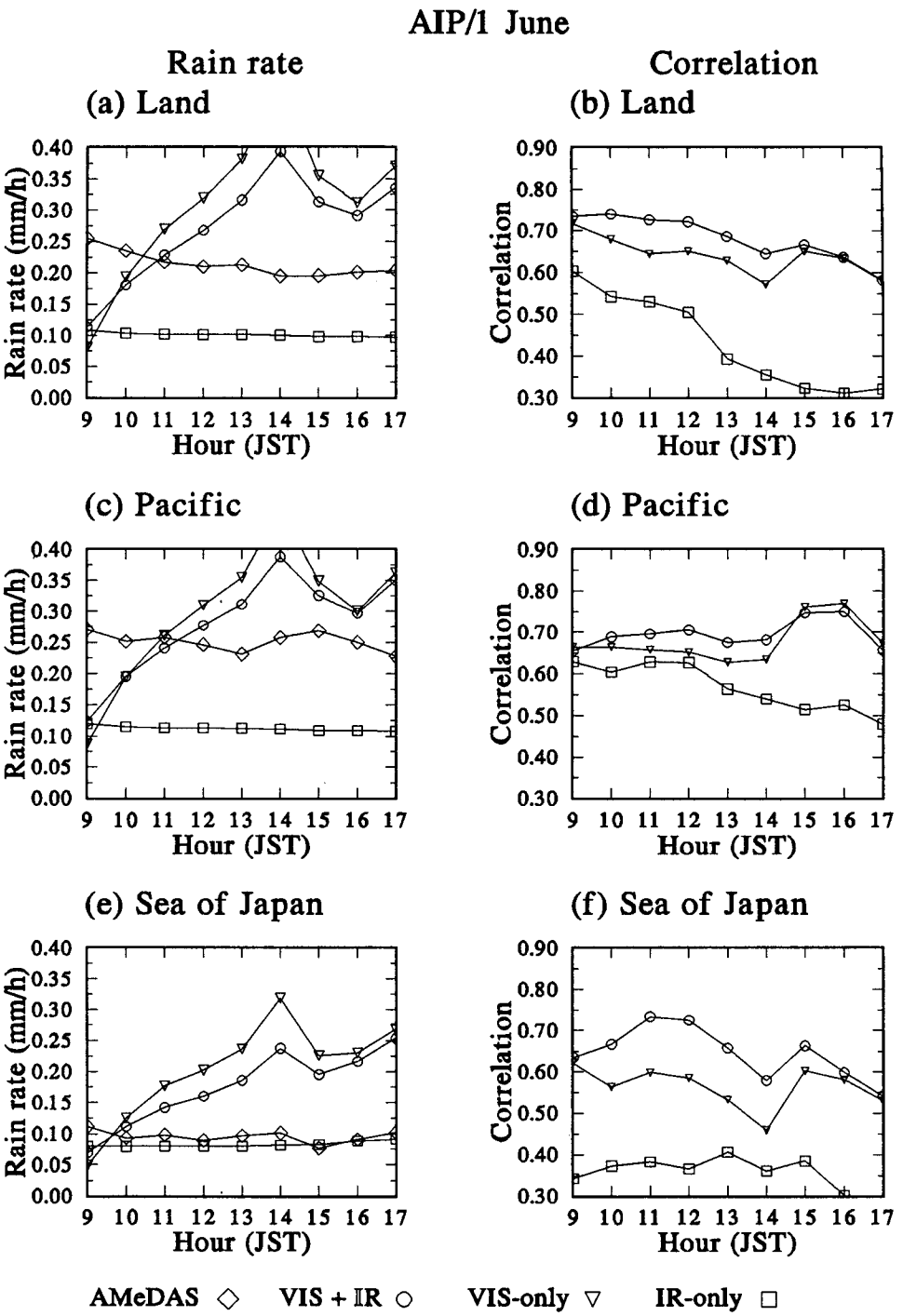

FIG. 13. (a), (c), and (e) Rain rate for AMeDAS (diamond), VIS + IR (circle), VIS-only (triangle), and IR-only (square) for June for land, Pacific, and Sea of Japan, respectively. (b), (d), and (f) Correlations between AMeDAS and the three rainfall estimation techniques.

daylight hours. It appears that the VIS data are better able to isolate the peaks and valleys in the rainfall data than are the IR. Of course there is a very big problem in getting the amounts right due at least in part to the normalization problem.

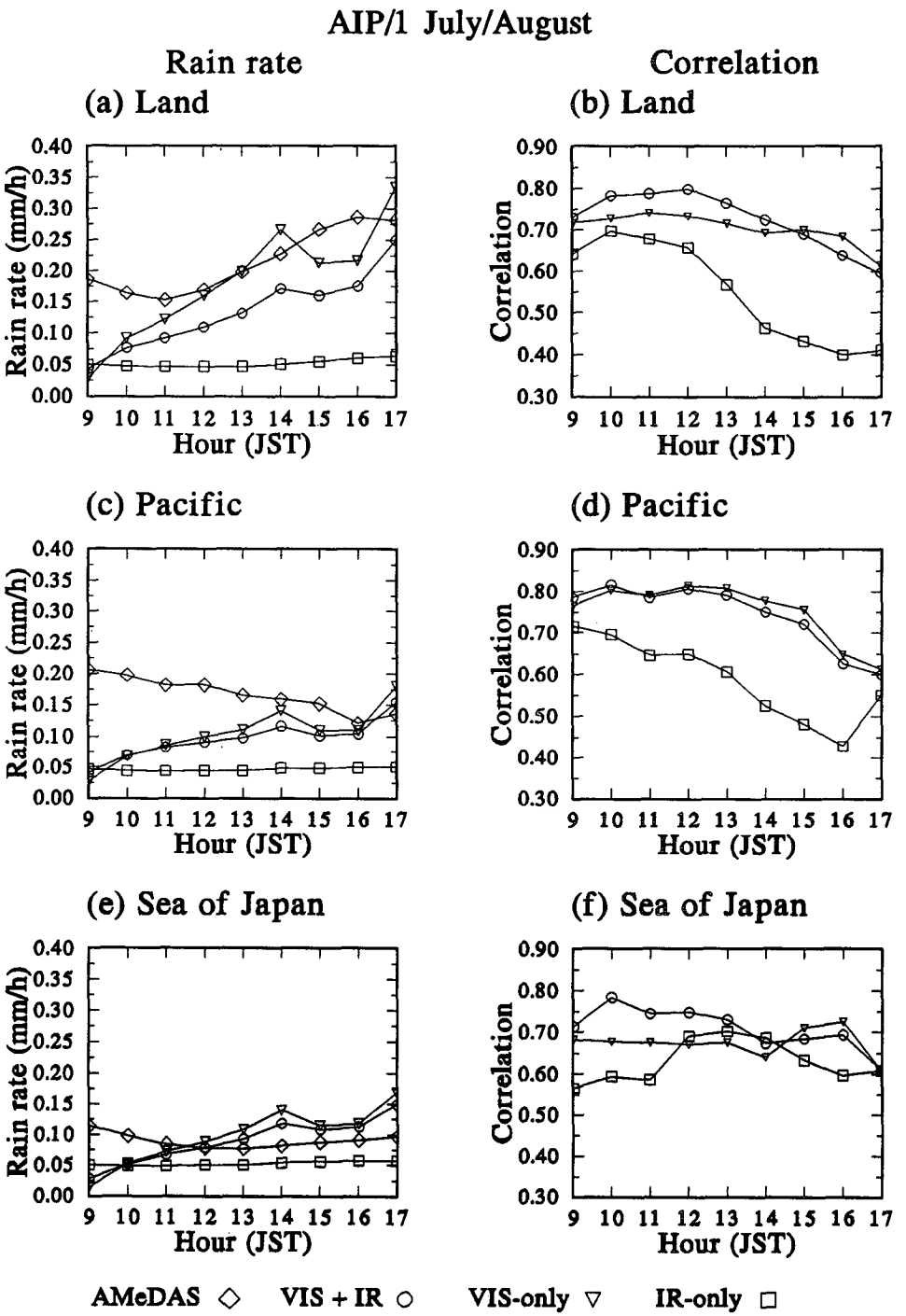

FIG. 14. As Fig. 13 but for July–August 1989.

In July/August the diurnal tendencies are even more pronounced. AMeDAS shows a clear afternoon rain-rate maximum over land but a slow decline during daylight hours over the Pacific. Over the Sea of Japan rain rates are much lower and there appears to be a broad minimum about midday. Again the IR-only shows a morning maximum for correlations over land and the Pacific. Over the Sea of Japan the IR-only is actually correlated better with AMeDAS than is the VIS-only for a few hours about midday.

We further subdivided the three areas along roughly latitudinal lines. There were no major differences since the southern areas, which received the most rain, dominate the statistics. From Fig. 13d it can be seen that the VIS-only correlations for June rise from morning to afternoon, while the IR-only correlations fall. We investigated this by comparing total rainfall with albedo and brightness temperatures for the periods 1000–1200 JST and 1400–1600 JST. Ninety percent of the rain volume occurred for albedos greater than 0.6 and close to 80% of the rain volume occurred for temperatures colder than 235 K for both periods. There was little difference between the morning and afternoon periods except for a slight tendency for rain to occur at slightly warmer temperatures in the afternoon. This would seem to support the idea that the rain-producing clouds change little from morning to afternoon in this area in June. The reasons for the differences in correlation from morning to afternoon are not obvious.

We did similar calculations for the southernmost land area for July/August. In this case there were very large morning to afternoon differences. In the morning about 40% of the rain fell with brightness temperatures less than 235 K, but this dropped to only 15% in the afternoon. The reason for this was that most of the heavy morning rainfall was due to a typhoon on 28 July. When this was removed from the dataset, the correlations fell for both techniques, slightly for the VIS-only (0.78 to 0.76) but greatly for the IR-only (0.65 to 0.49). On the rest of the days in July and August, rain was much lighter and fell from clouds that were warmer and less bright than those in June. This confirms the conclusion of Negri and Adler (1993) that rain was falling from warm convective clouds. It also appears that VIS data have some skill in estimating rainfall from such clouds.

The better correlation of RAINSAT during daylight hours prompted us to attempt daily and monthly rainfall accumulations based on daytime RAINSAT estimates only. We did this by simply multiplying the 8-h RAINSAT daylight accumulations (0900–1600 JST) by 3. When compared with AMeDAS, these RAINSATDAY accumulations for daily data exhibited spatial correlation coefficients similar to the full 24-h RAINSAT and superior to GPI. The Spatial correlation coefficients for the total June accumulation were 0.81 and 0.80 for RAINSAT and RAINSATDAY, respectively. RAINSATDAY had a slightly higher correlation (0.67) for July–August accumulations than did RAINSAT (0.64). These values give RAINSATDAY a higher correlation coefficient than any of the IR-only techniques submitted to AIP/1.

5. Conclusions

In this study we have examined the role of VIS data in improving rainfall estimates using VIS–IR techniques. We compared results from daytime RAINSAT (VIS + IR) with nighttime RAINSAT (IR-only) and with GPI. The RAINSAT algorithm generated estimates that were consistently the best correlated, among VIS–IR techniques, with the validating data during AIP/1. This paper shows that this result can be traced to the use of visible data by RAINSAT. We showed further that a VIS-only technique would have produced results comparable to the best of the VIS–IR techniques presented to AIP/1.

During daylight hours, the use of VIS data led to significantly better correlations with the validation data compared with IR-only techniques. During instances of widespread precipitation from cold, bright clouds, the correlations between the VIS-only and IR-only were similar, but in cases of precipitation from warmer clouds VIS-only had noticeably higher correlations. Thus VIS data may be especially useful in cases of warm rain.

The normalization of the VIS data using the cosine of the solar zenith angle did not completely remove the diurnal trend in apparent brightness. This must be due either to shortcomings of this normalization or to a real diurnal trend or both. More studies on the normalization of VIS data would be helpful in solving these problems.

Comparison of satellite data distributions from southern Ontario and Japan revealed that a significant relationship exists between the rain volume and the albedo of the clouds. This was especially pronounced during the July–August period when rain from convective clouds predominate over Japan.

The inclusion of visible data in VIS–IR techniques should result in improved estimates of convective rainfall during daylight hours. Exploitation of these relationships will likely require improvements in techniques for normalizing VIS data. Good visible calibration should be available from the GOES-Next satellite.

Acknowledgments. The authors wish to acknowledge useful discussions with Dr. Louis Garand and programming assistance from Hao Le and Ain Niitsoo. Eva Milewska provided Fig. 1. We would also like to thank the reviewers for their suggestions.

REFERENCES

Arkin, P. A., and B. N. Meisner, 1987: The relationship between large-scale convective rainfall and cold cloud over the Western Hemisphere during 1982–1984. *Mon. Wea. Rev.*, **115**, 51–74.

——, and P. Xie, 1994: The Global Precipitation Climatology Project: First Algorithm Intercomparison Project. *Bull. Amer. Meteor. Soc.*, **75**, 401–419.

Fujibe, F., 1988: Diurnal variations of precipitation and thunderstorm frequency in Japan in the warm season. *Pap. Meteor. Geophys.*, **39**, 79–94.

Fukui, E., Ed., 1977: *The Climate of Japan.* Elsevier, 317 pp.

Garand, L., 1989: Two automated methods to derive probability of precipitation fields over oceanic areas from satellite imagery. *J. Appl. Meteor.*, **28**, 913–924.

Grassotti, C., and L. Garand, 1994: Classification-based rainfall estimation using satellite and numerical forecast model fields. *J. Appl. Meteor.*, **33,** 159–178.

Hare, K., and M. K. Thomas, 1979: *Climate Canada.* 2d ed. Wiley Publishers of Canada, 230 pp.

Hogg, W. D., 1990: Comparison of some VIS/IR rainfall estimation techniques. *Fifth Conf. on Satellite Meteorology and Oceanography,* London, England, Amer. Meteor. Soc., 287–291.

JMA, 1993: *1990 Climatic Atlas of Japan.* Japan Meteorological Agency, 121 pp. and 104 plates.

King, P., 1990: On the relationship between GOES VIS and IR and radar rain rate. *Fifth Conf. on Satellite Meteorology and Oceanography.* London, England, Amer. Meteor. Soc., 150–155.

Lee, T. H., J. E. Janowiak, and P. A. Arkin, 1991: Atlas of products from the Algorithm Intercomparison Project. Part 1: Japan and surrounding oceanic regions June–August 1989. UCAR, NOAA/NMC/CAC, 131 pp.

Lovejoy, S., and G. L. Austin, 1979: The delineation of rain areas from visible and IR satellite data for GATE and mid-latitudes. *Atmos. Ocean,* **17,** 77–92.

Minnis, P., and E. F. Harrison, 1984: Diurnal variability of regional cloud clear-sky radiative parameters derived from GOES data. Part I: Analysis methods. *J. Climate Appl. Meteor.,* **23,** 993–1011.

Negri, A. J., and R. F. Adler, 1993: An intercomparison of three infrared rainfall techniques over Japan and surrounding waters. *J. Appl. Meteor.,* **32,** 357–373.

Ninomiya, K., and T. Akiyama, 1971: The development of the medium-scale disturbance in the Baiu front. *J. Meteor. Soc. Japan,* **49,** 663–677.

Rossow, W. B., and R. A. Schiffer, 1991: ISCCP cloud products. *Bull. Amer. Meteor. Soc.,* **72,** 2–20.